COLLIMATED ESCAPING VORTICAL POLAR e⁻e⁺ JETS INTRINSICALLY PRODUCED BY ROTATING BLACK HOLES AND PENROSE PROCESSES

Reva Kay Williams

Department of Astronomy, University of Florida, Gainesville, FL 32611

`revak@astro.ufl.edu`

ABSTRACT

In this paper, I present results from theoretical and numerical (Monte Carlo) *N-particle* fully relativistic 4-D analysis of Penrose scattering processes (Compton and $\gamma\gamma \longrightarrow e^-e^+$) in the ergosphere of a supermassive or stellar mass Kerr (rotating) black hole. Specifically, the escape conditions and the escaping orbits of the Penrose pair production ($\gamma\gamma \longrightarrow e^-e^+$) electrons are analyzed, revealing that these particles escape along collimated, jet geodesic trajectories encircling the polar axis. Such collimated vortical tightly wound coil-like trajectories of relativistic particles are inherent properties of rotating black holes. The helical polar angles of escape for these e^-e^+ pairs range from $\sim 40^o$ to $\sim 0^o.5$ (for the highest energy particles). These jet distributions appear to be consistent with the astrophysical jets of active galactic nuclei (AGNs) and galactic black holes, and suggest a mechanism for precollimation within the inner radius of the dynamically stable accretion disk.

Subject headings: acceleration of particles—black hole physics: jets: general—gravitation—relativity

1. Introduction

We now have observational evidence that black holes indeed exist in nature. They are at the cores of quasars and other active galactic nuclei (AGNs) as well as sources in our Galaxy, commonly referred to as microquasars or galactic black holes. Many of these sources are associated with polar jets emanating from their cores. Black holes were theoretically predicted from Einstein's theory of general relativity. Theoretical and numerical calculations (Williams 1991, 1995, 1999, 2001, 2002a, 2002b, 2003), described briefly below, show that

Penrose (1969) gravitational-particle scattering processes are sufficient to describe energy-momentum extraction from a rotating Kerr (1963) black hole, from radii within the marginal stable orbit ($r \lesssim r_{\mathrm{ms}} \simeq 1.2M$, in gravitational units: $c = G = 1$; $a/M = 0.998$, where a is the angular momentum per unit mass parameter and M is the mass of the black hole), while electromagnetic interactions or magnetohydrodynamics (MHD) appear to govern the "flow" of polar jets of the extracted particles, escaping away from the central source, out to the observed distances, as suggested by observations (Junor, Biretta, & Livio 1999).

In the primary paper cited above (Williams 1995), theoretical model calculations involving Monte Carlo computer simulations of Compton scattering and electron-positron (e^-e^+) pair production processes in the ergosphere of a supermassive ($\sim 10^8 M_\odot$) rotating black hole are presented. Particles from an accretion disk surrounding the rotating black hole fall into the ergosphere and scatter off particles that are in bound equatorially and nonequatorially confined orbits. The accretion flow is assumed to be of the form of the so-called *two-temperature* bistable disk model, in which the disk can in principle exist in two phases: a thin disk (Novikov & Thorne 1973) and/or ion torus (Lightman & Eardley 1974; Shapiro, Lightman, & Eardley 1976; Eilek 1980; Eilek & Kafatos 1983), where the electrons and protons (or ions) can have separate temperatures of up to $\sim 10^9$ K and $\sim 10^{12}$ K, respectively. Note that disk models of this sort are also referred to as thin disk/ion corona models, and more recently, the ion corona has been called an advection dominated accretion flow (ADAF; Mahadevan, Narayan, & Krolik 1997). The Penrose mechanism, in general, allows rotational energy of a Kerr black hole (KBH) to be extracted by scattered particles escaping from the ergosphere to large distances from the rotating black hole. The results of these model calculations show that the Penrose mechanism is capable of producing the astronomically observed high energy particles ($\sim$ GeV) emitted by quasars and other AGNs. This mechanism can extract hard X-ray to γ-ray photons from Penrose Compton scatterings of initially low energy soft X-ray photons by target orbiting electrons in the ergosphere. The Penrose pair production ($\gamma\gamma \longrightarrow e^-e^+$) processes allow relativistic e^-e^+ pairs to escape with energies up to ~ 4 GeV, or greater depending on the form of the accretion disk; these pairs are produced when infalling low energy photons collide with bound, highly blueshifted photons at the *photon orbit*. This process may very well be the origin of the relativistic electrons inferred from observations to emerge from the cores of AGNs. Importantly, these model calculations show that the Lense-Thirring effect (Thirring & Lense 1918), i.e., the dragging of inertial frames into rotation, inside the ergosphere, caused by the angular momentum of the rotating black hole, results in a gravitomagnetic force being exerted on the scattered escaping particles. This force (which is the gravitational analog or resemblance of a magnetic force) produces asymmetrical particle emissions in the polar direction, above and below the equatorial plane, consistent with the asymmetrical or one-sided jets observed in

radio strong AGNs (Williams 2002a, 1999)[1]. The dragging of inertial frames also causes the Penrose escaping particles to escape along vortical trajectories (as discussed in the following paragraphs).

These Penrose processes can apply to any size rotating black hole and, in general, to any type of relativistic elementary particle scattering energy-momentum exchange process, inside the ergosphere, allowing particles to escape with rotational energy-momentum from the KBH. Even in the context of MHD, according to the guiding center (Landau & Lifshitz 1975) approximation, the single-particle approach is essential close to the black hole (de Felice & Carlotto 1997; Karas & Dovčiak 1997; de Felice & Zonotti 2000), i.e., the behavior of individual particles moving along geodesics in the strong central gravitational force field is also that of the bulk of fluid elements. This suggests that even though a MHD simulation is not performed in this present paper, the results will be valid for the trajectories of particle flows and e^-e^+ pairs produced near the black-hole event horizon. Nevertheless, the Penrose analysis presented here should be considered in the context of a full-scale relativistic MHD simulation. However, because of the proximity of the Penrose processes to the horizon, and the dominating effect of gravity, the resulting trajectories are expected to be approximately the same in the MHD regime.

In the model calculations summarized above, in which energy-momentum is extracted from a rotating black hole, it is found that particles escape with relativistic velocities along vortical trajectories, above and below the equatorial plane, with small helical angles of escape, implying strong coil-like vortex plasma collimation (Williams 2001, 2002b). Thus, from these model calculations, it appears that the rotating black hole naturally produces particle trajectories collimated about the axis of symmetry, i.e., the polar axis. Such vortical orbits or trajectories have been discussed by some other authors (de Felice & Calvani 1972; de Felice & Curir 1992; de Felice & Carlotto 1997; de Felice & Zanotti (2000); see also Bičák, Semerák, & Hadrava 1993; Karas & Dovčiak 1997). Their independent findings, deduced from the geodesic properties of the Kerr metric, and referred to as geometry induced collimation, can serve as confirmation of Williams' (1991, 1995) theoretical and numerical calculated results, or vice versa.

In this paper, I examine the escape conditions and the resulting four-momentum vectors of the Penrose pair production ($\gamma\gamma \longrightarrow e^-e^+$) processes, showing that the particles indeed escape to infinity in the form of vortical jets intrinsically collimated about the polar

---

[1]Figures 1(c) and 1(d) of Williams (1999) are incorrect. Figures 4(e) and 4(h), respectively, of Williams (2002a) are the correct figures, where in Figure 4(h) the target electrons have both positive and negative equal absolute value polar coordinate angular momenta.

axis, because of the frame dragging of spacetime inside the ergosphere of the KBH. Importantly, we shall see that these $e^- e^+$ pairs escape without any appreciable interaction with the dynamically stable accretion disk particles. Now, although most of the Penrose Compton scattered photons escape along vortical trajectories as well, we are concerned, in this paper, only with the Penrose pair production ($\gamma\gamma \longrightarrow e^- e^+$) electrons, because these are the particles that compile the main constituents of the observed jets, being responsible for the synchrotron radiation and Doppler boosting (giving rise to superluminal motion). I refer the reader to the above references, particularly Williams (1995), for a thorough description of the "Penrose-Williams" (Williams 2002b) processes discussed in this present paper.

2. Escape Conditions and Vortical Orbits

After the scattering events, not all of the particles escape to infinity. A set of escape conditions must be applied to see if a particular particle escapes from the gravitational potential well of the black hole [see Williams (1995) and references therein for further descriptions of the escape conditions]. It is known that outside the event horizon, the orbit of a photon (or an unbound material particle with $E/\mu_o > 1$), may have one or no radial turning points for which $P_r \to 0$ (Piran & Shaham 1977; Williams 1995), where E is the energy of the particle as measured by an observer at infinity; μ_o is the rest mass energy; and P_r is the radial component of the covariant four-momentum vector $[P_\mu = (P_r, P_\Theta, P_\Phi, -E)]$. Let L define the conserved azimuthal coordinate angular momentum ($= P_\Phi$), then if E/L for that particle lies in the range

$$\frac{E}{L} \leq \frac{E_{\text{orb}}}{L_{\text{orb}}}, \tag{1}$$

for a direct orbit not confined to the equatorial plane [$Q > 0$; Q is the so-called Carter constant of motion (Carter 1968):

$$Q = P_\Theta^2 + \cos^2\Theta\left[a^2\left(\mu_o^2 - E^2\right) + \frac{L^2}{\sin^2\Theta}\right], \tag{2}$$

where the value of Q is zero for particles whose motions are confined to the equatorial plane], there will be one turning point; otherwise, there will be none, where E_{orb} is the iso-energy orbit: the circular orbit of equal energy at constant radius $r = r_{\text{orb}}$, a potential turning point, and L_{orb} is the corresponding azimuthal angular momentum. Another independent condition for the existence of a turning point for which $P_r \to 0$ is

$$\frac{Q}{E^2} \geq \frac{Q_{\text{orb}}}{E_{\text{orb}}^2}, \tag{3}$$

where Q_{orb} is the corresponding Q value of the iso-energy orbit. [Note, a bound circular orbit is considered as an orbit with a "perpetual" turning point (see Williams 1995).] In

equations (1) and (3), $E_{\rm orb}$ and $L_{\rm orb}$ are the conserved orbital energy and azimuthal angular momentum as measured by an observer at infinity, given by (Williams 1995)[2]

$$E = \left(\frac{r^2 L^2 + D + F}{G} \right)^{1/2},$$ (4)

and

$$P_\Phi = L = \left[\frac{-J - (J^2 - 4IK)^{1/2}}{2I} \right]^{1/2},$$ (5)

where

$$I \equiv \frac{\tilde{A}^2 r^4}{G^2} - \frac{r^2}{G}(2\tilde{A}C + B^2) + C^2,$$

$$J \equiv \frac{(D+F)}{G}\left[\frac{2\tilde{A}^2 r^2}{G} - 2\tilde{A}C - B^2 \right] + 2\Delta(r^2\mu_o^2 + Q)\left[C - \frac{\tilde{A}r^2}{G} \right],$$

$$K \equiv \frac{\tilde{A}^2}{G^2}(D+F)^2 - \frac{2\tilde{A}\Delta}{G}(r^2\mu_o^2 + Q)(D+F) + \Delta^2(r^2\mu_o^2 + Q)^2;$$

and

$$\tilde{A} \equiv [(r^2 + a^2)^2 - a^2\Delta],$$
$$B \equiv 4Mar,$$
$$C \equiv \Delta - a^2,$$
$$D \equiv (3r^4 - 4Mr^3 + a^2r^2)\mu_o^2,$$
$$F \equiv (r^2 - a^2)Q,$$
$$G \equiv 3r^4 + a^2r^2,$$

for direct orbits of constant radius r, where $\Delta \equiv r^2 - 2Mr + a^2$.

Upon applying equations (1) and (3) to the Penrose pair production ($\gamma\gamma \longrightarrow e^-e^+$) electrons, for $E \equiv E_\mp$, $L \equiv L_\mp$, and $Q \equiv Q_\mp$, where $E_\mp$, $L_\mp$, $Q_\mp$ are the parameters for a Penrose pair produced electron, we find that most satisfy the condition to have a turning point at the iso-energy orbit $E_{\rm orb}$, with $E_\mp = E_{\rm orb}$ and $L_\mp \gtrsim L_{\rm orb}$ at radii $r_{\rm orb} \sim r_{\rm mb}$ (the last bound orbit for a material particle, deep within the ergosphere), before escaping to infinity along vortical orbits about the polar axis, satisfying (Williams 1995)

$$0 < \frac{Q_\mp}{E_\mp^2} < \frac{Q_{\rm orb}}{E_{\rm orb}^2},$$ (6)

or $Q_\mp < Q_{\rm orb}$, implying no turning point in $(P_\mp)_\Theta$, i.e., $(P_\mp)_\Theta \nrightarrow 0$, yet $(P_\mp)_r \rightarrow 0$ at $r_{\rm orb}$ according to satisfaction of equation (1), where $(P_\mp)_\Theta$ is the polar coordinate angular momentum of a Penrose produced electron.

---

[2] Note the typographic error in equation (A17) of Williams (1995): μ_0 is supposed to be μ_0^2.

3. Discussion

That the Penrose produced e^-e^+ pairs escape to infinity along vortical trajectories without any appreciable interaction with stable accretion disk particles can be seen in the momentum spectra of Figures 1, 2 (for a supermassive KBH), and Figure 3 (for a "micromassive" KBH), as explained in the paragraphs below. Note, in gravitational units ($G = c = 1$) such distribution spectral plots for the same initial energies are approximately the same irrespective of the mass of the black hole adopted to make the plot (see Williams 2002b). The Penrose pair production processes used to calculate Figures 1, 2, and 3 are for an idealized configuration with the purpose to simply show the effect of the inertial frame dragging [produced by the gravitational field of the spinning black hole, i.e., its gravitomagnetic field (Williams 1999; 2002a)], and not an attempt to connect the calculations to detailed observations. Nevertheless, the initial energies used for these Penrose processes are based on energies found to exist in relativistic accretion disk models (Novikov & Thorne 1973; Eilek 1980; Eilek & Kafatos 1983) for black hole masses $10^8 M_\odot$ and $30 M_\odot$, and the expected blueshift in orbital energies: increased by the factor $e^{-\nu} = \sqrt{-g^{tt}} \simeq 52$ at the photon orbit (Williams 1995), where g^{tt} is the contravariant diagonal time component of the Kerr metric in Boyer-Lindquist (1967) coordinates; such initial energies yield final results consistent with general observed jet particle energies. The initial incident photons, indicated by the subscript $\gamma 1$, are assumed to infall radially along the equatorial plane [$(P_{\gamma 1})_r < 0$, $L_{\gamma 1} = Q_{\gamma 1} = 0$), with energies $E_{\gamma 1} = 0.03$ MeV for Figures 1 and 2; $E_{\gamma 1} = 0.0035$ MeV for Figure 3. These incident photons are allowed to collide with highly blueshifted target photons that orbit at the photon orbit $r = r_{\rm ph} = 1.074M$, in nonequatorially confined trajectories, which repeatedly cross (i.e., pass through) the equatorial plane in "spherical-like" orbits that reach certain latitudinal angles (Wilkin 1972). The collision is assumed to take place when the target photon passes through the equatorial plane. The initial orbital parameters for the target photons, indicated by the subscript $\gamma 2$, are given by equations (4) and (5) for a particular $Q_{\gamma 2}$. Specifically, the target photon orbits can be populated by prior Penrose Compton scattering (Williams 1995; 2002b), and probably by proton-proton scatterings of neutral pions that decay ($\pi^0 \longrightarrow \gamma\gamma$), occurring in "hot" ADAFs (Eilek & Kafatos 1983; Mahadevan, Narayan, & Krolik 1997), assuming some of the π^0-decay photons are created with appropriate Q values and energies to become bound at the photon orbit (Williams 1995, 2002a). Now, in a realistic situation the incident and target particles are not constrained to this idealized configuration, but this configuration, including the range of initial energies used (see also captions of Figs. 1, 2, and 3), is most efficient and allows maximum energy-momentum extraction (Williams 1995).

Figures 1a, 2a, and 3a show the azimuthal momenta $L_\mp$ of the Penrose pair production ($\gamma\gamma \longrightarrow e^-e^+$) versus the energy $E_\mp$ of the escaping electron pairs after 2000 events [each point (i.e., tiny dot) represents an escaping particle resulting from the events]. In general,

since the energy E as measured by an observer at infinity is linearly proportional to the azimuthal angular momentum L in the transformation laws, from the local nonrotating frame to the observer's frame at infinity [compare eqs. (2.7c) and (2.7d) or (3.89a) and (3.89d) of Williams 1995], and since there is a linear relationship between E and L in the Boyer-Lindquist coordinate frame, as can be seen in Figures 1b, 2b, and 3b (compare also equation [4]), which is apparently transferred to the scattered particles, the scatter plots (Figs. 1a, 2a, 3a) representing the approximately 2000 escaping electrons per plot appear linear.

Figures 1b, 2b, and 3b show the azimuthal coordinate momentum versus energy of the e^-e^+ pairs, superimposed on the azimuthal coordinate momentum versus energy, orbital parameters, of an electron orbit not confined to the equatorial plane (Wilkins 1972), at $r_{\rm mb}$ and $r_{\rm ms}$, the radii of marginally bound and marginally stable orbits, respectively. The conserved orbital parameters E and L for the nonequatorially confined orbits (for massless and material particles), which reduce to the forms of Bardeen, Press, Teukolsky (1972) for $Q = 0$, as measured by an observer at infinity, are given by equations (4) and (5). Notice on Figures 1b, 2b, and 3b that for $E_\mp = E_e \equiv E_{\rm orb}$ at $r_{\rm mb}$, $r_{\rm ms} \equiv r_{\rm orb}$ most of the escaping e^-e^+ pairs have $L_\mp > L_e$, indicating turning points inside the inner radius of the stable accretion disk ($\sim r_{\rm ms}$); and some, particularly the higher energy pairs, have turning points inside $r_{\rm mb}$. Moreover, compare Figures 1b, 2b, and 3b over the total energy range to see that the curves for $r_{\rm ms}$ and $r_{\rm mb}$ do not merge into one curve at lower energies; they only appear to on Figures 1b and 2b. This, as well as the satisfaction of the turning point condition stated above (according to equation [1]) at $r \lesssim r_{\rm mb}$ and/or $\lesssim r_{\rm ms}$, can clearly be seen when comparing Figures 4 and 5, which show specific intervals for the cases displayed in Figures 1b and 2b.

Notice also that, the display in Figures 1c, 2c, and 3c, showing $|(P_\mp)_\Theta| < |(P_e)_\Theta|$ for $E_\mp = E_e \equiv E_{\rm orb}$ at $r_{\rm mb}$, $r_{\rm ms} \equiv r_{\rm orb}$ for most of the escaping e^-e^+ pairs[3], means that these electrons escape to infinity along vortical trajectories, with helical angles of escape, measured relative to the equatorial plane, $\delta_\mp = |90° - \Theta_\mp| \sim 60°$ to $0°.5$, $\delta_\mp \sim 9°$ to $0°.5$, and $\delta_\mp \sim 6°$ to $0°.5$, for the electrons displayed in Figures 1, 2, and 3, respectively (see Fig. 6; see also Williams 2002b, 2002a).

Finally, notice that in Figure 1c, some of the e^-e^+ pairs with $E_\mp \lesssim 2.5$ MeV do not escape and can possibly become bound, i.e., populate the orbits, at $r_{\rm mb}$ or $r_{\rm ms}$ for "later" Penrose Compton scattering events, involving these nonequatorially confined electrons as

---

[3]The absolute value brace are included to emphasize that we are comparing the magnitude of the polar coordinate angular momentum.

targets (Williams 1995, 2002b). This shows that these Penrose processes and the accretion disk assumed (Williams 1995) can compile a self-consistent model producing the three general spectral high energy regimes observed in all AGNs, more or less (e.g., compare Figure 8 of Williams 2003). That is, for a particular self-consistent case, somewhat *similar* to that of Figure 1, from prior Penrose Compton scattering of initial photons (0.03 MeV) by equatorially confined electron targets at $r_{\rm mb}$, the final inward scattered photons ~ 330 keV, with turning points after being blueshifted by a factor of $e^{-\nu} \simeq 52$ (Williams 2002a), can populate the photon orbit for Penrose pair production ($\gamma\gamma \longrightarrow e^- e^+$), which in turn yields electrons that can populate the nonequatorially confined target orbits: with energies up to ~ 3 MeV, similar to that seen in Figure 1c, for subsequent Penrose Compton scattering. In this self-consistent case, however, $E_{\mp}$ can extend up to ~ 17 MeV (compare Fig. 1). Note, the population of the target particle orbits and accretion disk properties are discussed in details in Williams (1995, 2002a, 2002b, 2003).

The helical angles of escape stated above (compare Fig. 6), and given analytically by

$$\delta = \arccos\left[\frac{-T + \sqrt{T^2 - 4SU}}{2S}\right]^{1/2},\tag{7}$$

where

$$\begin{aligned}
S &\equiv a^2(\mu_o^2 - E^2), \\
T &\equiv Q + a^2(E^2 - \mu_o^2) + L^2, \\
U &\equiv -L^2
\end{aligned}$$

[as derived from the "Carter constant" of motion by letting $P_\Theta \longrightarrow 0$ (see equation [2]; see also Piran & Shaham 1977), where $\Theta_{\mp} = 90° \pm \delta_{\mp}$ for escaping below "+" or above "−" the equatorial plane], suggest that the particles escape to large distances along coil-like geodesics conglomerated in the form of collimated swirling current plasma polar jets, with energy-momentum of the KBH transferred from the highly blueshifted frame dragged scattering events. Now, a test particle moves on a geodesic in a gravitational field if it is not acted on by some external force, but if the parameters such as energy and angular momentum vary with time, then forces are present that can destroy the geodesic character of the motion. But the geodesic character of a trajectory, however, can be approximately saved if the time scale of a significant variation of the physical parameters, say τ_{var}, is longer than the dynamical time, τ_{dyn}, associated with a geodesic trajectory (de Felice & Carlotto 1997). This means that, if the orbital parameters vary slightly so as to preserve the initial Θ angle (i.e., the emission angle of the particle above or below the equatorial plane), then under suitable conditions, say in a suitable electromagnetic field, we obtain a net axial collimation.

Calculations by de Felice & Carlotto (1997); Karas & Dovčiak (1997) suggest that the average dynamical time associated with the vortical geodesics is sufficiently short to give confidence that the average time of a significant variation of the physical parameters, due to dissipative or accelerating processes, is long enough to ensure the geodesicity condition on outgoing vortical orbits. This then can possibly permit the maintenance of the intrinsic collimation of the Penrose scattered particles by the KBH, particularly because of the sturdiness or stiffness (de Felice & Carlotto 1997) of the coil-like structure of the geodesics. Moreover, their calculations also show that for a Lorentz force acting on a charge particle near the event horizon, for a $10^8 M_\odot$ KBH, inertia and gravity dominate over electromagnetic disturbance.

For completeness, the overall difference in the distributions of the polar angles of escape, displayed in Figure 6, is a general relativistic effect due to the gravitomagnetic (GM) force field acting on the momentum of individual particles, resulting in an "alteration" of the incoming and scattering angles. The resultant force in the polar direction, as conveyed in the spectra of Figure 6, depends largely on the counterbalance between the dynamics of the nonequatorially confined target photons' orbits (with latitudinal angles $\lesssim 0°.5$ about the equatorial plane) and the GM force. Note, an important feature of the GM field (caused by the angular momentum of the rotating black hole) is the production of symmetrical and asymmetrical polar jets: appearing to break the expected reflection symmetry of the Kerr metric, above and below the equatorial plane (Williams 2002a). The general shapes of the spectra are not the same because the energy-momenta of the initial and escaping particles, in the three cases (Figs. $6a-6c$) are different; therefore, the GM force ($\mathbf{F}_{\mathrm{GM}} = \overset{\leftrightarrow}{\mathbf{H}} \cdot \mathbf{p}$), acting proportional to the momentum ($\mathbf{p}$) of a particle, will be different, where $\overset{\leftrightarrow}{\mathbf{H}}$ is the GM tensor (Thorne, Price, & Macdonald 1986). The GM force behaves in some degree like a "Coriolis force," acting on the momentum of particles in the local inertial frame that has been dragged into rotation. This can be somewhat understood by looking at the GM force component in the polar direction:

$$(F_{\mathrm{GM}})_\Theta \propto (H^r P_\Phi - \tilde{H}^\Phi P_r); \tag{8}$$

with

$$
\begin{aligned}
H^r &\leq 0 \ \text{ for } \ \Theta \leq 90°, \\
H^r &\geq 0 \ \text{ for } \ \Theta \geq 90°, \\
\tilde{H}^\Phi &> 0 \ \text{ for } \ \Theta \leq 90° \ \text{ and } \ \Theta > 90°,
\end{aligned} \tag{9}
$$

as defined by the components of the GM tensor for $r \sim r_+$, where it appears that the spacetime frame dragging is so severe that the GM field lines are distorted into the direction of rotation, producing the nonzero $\tilde{H}^\Phi$ term (Williams 2002a). Notice in equation (8), using

equation (9), that the first term maintains equatorial reflection symmetry, while the second term introduces asymmetry; this second term is expected to exist effectively only near the event horizon (r_+), i.e., inside the ergosphere: the region of importance for the Penrose mechanism to operate. A general analysis of equations (8) and (9) reveals the following conditions:

1. At $\Theta = 90°$, $P_r < 0$ or $P_r > 0$, the force on the particle will be $(F_{\rm GM})_\Theta > 0$ or $(F_{\rm GM})_\Theta < 0$, respectively.

2. At $\Theta > 90°$, $P_r > 0$, $P_\Phi > 0$, the force on the particle will be $(F_{\rm GM})_\Theta > 0$ for $H^r P_\Phi > \tilde{H}^\Phi P_r$, and $(F_{\rm GM})_\Theta < 0$ for $H^r P_\Phi < \tilde{H}^\Phi P_r$.

3. At $\Theta < 90°$, $P_r > 0$, $P_\Phi > 0$, the force on the particle will be $(F_{\rm GM})_\Theta < 0$.

We now use the three conditions above to explain the escaping particle distribution in the individual spectra of Figure 6. The momentum components (P_Φ, P_r) and the polar angle (Θ) are to be compared with that of the initial and escaping particles. In the case of the lowest energy (Fig. 6c; see also Fig. 3) target $(E_{\gamma2} \simeq 3.387$ MeV) and incoming $(E_{\gamma1} = 0.0035$ MeV) photons, the initial asymmetry, favoring the positive $\hat{\bf e}_\Theta$ direction, is established by the GM field acting on the radially infalling photons according to condition 1. The outward radial momenta of the escaping electrons with $90° \lesssim \Theta_\mp \lesssim 90°$, according to conditions 1−3, are not large enough to overcome the force produced by $(F_{\rm GM})_\Theta > 0$; therefore, the asymmetry remains. For the lowest energy escaping electrons, the GM force dominates over the dynamics of the target photons, resulting in helical angles of escape $\delta_\mp > 0°.5$ for most of the escaping electrons. Also, the H^r component has a larger absolute value for a particle with a larger $\delta_\mp$ (Williams 2002a), thus contributing to the distribution being forced away from the equatorial plane according to conditions 2 and 3 (compare eqs. [8] and [9]). Finally, in this particular case, as the energy of the escaping electrons increases, the GM force dominates less and less, while the orbital dynamics of the target photons begin to dominate, producing smaller $\delta_\mp$ values, consistent with the latitudinal angles of the target photons (which are $\lesssim 0°.5$).

In the case of the somewhat higher energy (Fig. 6a; see also Fig. 1) target $(E_{\gamma2} \simeq 13.54$ MeV) and incoming $(E_{\gamma1} = 0.03$ MeV) photons, the initial asymmetry, favoring the positive $\hat{\bf e}_\Theta$ direction, caused by the GM field acting on the radially infalling photons according to condition 1 appears to be approximately balanced by $(F_{\rm GM})_\Theta < 0$ according to conditions 2 and 3, except at the very highest energy of the escaping electron pairs, where $(F_{\rm GM})_\Theta > 0$ dominates according to condition 2, producing asymmetry. For most of the escaping electrons, the GM force dominates over the dynamics of the target photons, resulting

in helical angles of escape as high as $\delta_{\mp} \sim 60°$ according to conditions 2 and 3. Nevertheless, as the energy of the escaping electrons increase, the orbital dynamics of the target photons begin to dominate, producing smaller $\delta_{\mp}$ values.

In the case of the highest energy (Fig. 6b; see also Fig. 2) target ($E_{\gamma 2} \simeq 2146$ MeV) and incoming ($E_{\gamma 1} = 0.03$ MeV) photons, the asymmetry, favoring the positive $\hat{\mathbf{e}}_{\Theta}$ direction, caused by the GM field acting on the the radially infalling photons according to condition 1 and the high energy escaping electrons according to condition 2, where $(F_{\mathrm{GM}})_{\Theta} > 0$ dominates for $H^r P_{\Phi} > \tilde{H}^{\Phi} P_r$ (recall that P_{Φ} increases with increasing E), appears to dominate over $(F_{\mathrm{GM}})_{\Theta} < 0$ in conditions $1-3$. Also, except for the relatively very lowest energy of the escaping pairs, the orbital dynamics of the target photons appear to dominate over the GM force, as the escaping energy increases, producing predominantly electrons with $\delta_{\mp} \lesssim 1°$.

Note, in these Penrose processes, the GM force is inherently tied to the overall scattering process through the Kerr metric. That is, just as we do not have to calculate separately the gravitational force on the scattered particles due to the mass M of the KBH, we do not have to calculate separately the GM force on the scattered particles due to the angular momentum J of the KBH. The GM force, however, is given here separately only to show how it relates to the final four-momenta of the scattered particles, in an effort to explain the major difference of spectral distributions displayed in Figure 6.

4. Conclusions

In this paper, I have shown that the Penrose pair production ($\gamma\gamma \longrightarrow e^- e^+$) electrons, of processes occurring at the photon orbit r_{ph}, escape to infinity along vortical trajectories about the polar axis, without any appreciable interaction with the stable accretion disk particles (which are located at $r \gtrsim r_{\mathrm{ms}}$). This is also expected to be true for the Penrose Compton scattered escaping photons that have inward directed radial momenta with turning points at $r \sim r_{\mathrm{ph}}$, escaping along vortical orbits concentric to the polar axis (Williams 2001, 2002b). On the other hand, since the Penrose Compton scattering processes occur at radii $r_{\mathrm{mb}} \lesssim r \lesssim r_{\mathrm{ms}}$ the scattered photons with positive radial momenta probably have appreciable interaction with the inner region of the accretion disk, as suggested by the broad Fe Kα emission line at ~ 6 keV observed in the bright Seyfert 1 galaxy MCG—6-30-15 (Wilms et al. 2001); see the qualitative description in Williams (2002b). Details concerning MCG—6-30-15 will be investigated in a future paper.

Overall, these vortical trajectories of escaping particles suggest that the KBH is responsible for the precollimation (de Felice & Curir 1992; de Felice & Carlotto 1997; de Felice

& Zanotti 2000; see also Bičák, Semerák, & Hadrava 1993; Karas & Dovčiak 1997) of the observed jets of relativistic particles, emanating from the cores of objects powered by black holes (compare Junor, Biretta, & Livio 1999). Note, the coil-like collimation of the vortical orbits, presented here, and those of the Penrose Compton scattering processes, are investigated in further details elsewhere. Further investigations of this precollimation will include the self-induced dynamo magnetic field associated with the vortical orbiting escaping Penrose produced ($\gamma\gamma \longrightarrow e^- e^+$) pairs; such a field could be an important contribution to the observed synchrotron emission as well as in maintaining collimation. Recent polarization measures (e.g., see Homan 2004 and references therein) appear to be consistent with the dynamics and kinematics of these vortical polar trajectories of escaping electrons. The degree to which the above statement applies consistently, with the interpretation that the observed transverse rotation-measure gradients across the jets (Gabuzda & Murray 2003) are due to an intrinsic helical magnetic field structure associated with the accretion disk, must be looked at in detail. The best-case scenario would be for the magnetic field of the accretion disk to assist in further collimating and accelerating the Penrose produced relativistic jet particles as they escape from the black hole out to observed distances.

In comparison with some MHD energy extraction models, of the Blandford-Znajek (1977) and Blandford-Payne (1982) type, we find the following. Firstly, because of the proximity of the Penrose pair production ($\gamma\gamma \longrightarrow e^- e^+$) processes (Williams 1995) to the event horizon, i.e., occurring at the photon orbit r_{ph} inside the marginally bound orbit r_{mb} (the last radius for any bound material particle before it falls directly into the black hole), the accretion disk magnetic field, proposed to be frozen to the plasma particles (e.g., Koide et al. 2002; Koide 2003; Meier, Koide, & Uchida 2001), is expected to have a negligible effect on these pair production processes, even without considering that the existences of such magnetic fields or "flux tubes" near the event horizon are inconsistent with general relativistic findings by Bičák (2000) and Bičák & Ledvinka (2000). These findings reveal that such fields, if aligned with the rotation axis, will be expelled from the horizon or redshifted away, for a rapidly rotating black hole (i.e., a near extreme KBH). Now based on these findings, it is probably safe to say that the disk magnetic field may have little, if any, effect on the Penrose Compton scattering processes (Williams 1995), particularly those occurring at $\sim r_{\mathrm{mb}}$, the radii first to be populated by the target electrons (Williams 2002b) and where the most energy would be extracted for a specific Q_e value [compare the bound electron orbits displayed in Figs. 1c and 3c; see also Fig. 1(b) of Williams 1995]. The radius of marginally bound orbit r_{mb} is closer to the event horizon ($\Delta r \equiv r_{\mathrm{mb}} - r_+ \simeq 0.026M$) than it is to r_{ms} ($\Delta r \equiv r_{\mathrm{mb}} - r_{\mathrm{ms}} \simeq 0.111M$), where $r_+ \simeq 1.063M$ for $a = 0.998M$ (Bardeen et al. 1972).

Secondly, the main advantage of the Penrose-Williams processes, over such Blandford-Znajek (1977) and Blandford-Payne (1982) type models, is that the Penrose-Williams grav-

itational energy-momentum extraction processes occur independently of a magnetic field, while producing highly relativistic particles that escape to infinity along intrinsically collimated vortical trajectories in the form of symmetrical or asymmetrical jets, because of the inertial frame dragging. Another feature of these processes is that most of the energy extracted is gravitational binding energy with only a small fraction of the scattered particles having final negative energies (up to $\sim 30\%$ of the Penrose Compton scattered photons and up to $\sim 10\%$ of the Penrose pair produced electrons, occurring only in the lowest energy-momentum scattering processes), which means that the angular momentum of the black hole will not decrease significantly in these processes. The lifetime of these processes is expected to be indefinite as long as there is matter to be accreted, since positive energy-momentum particles are also scattered into the KBH. The resulting escaping plasma jets are expected to generate a self-induced dynamo magnetic field, as stated above, in the form of a polar solenoid-like field, which could possibly magnetically confine and further assist in acceleration, collimation processes, as well as producing observed synchrotron radiation. Importantly, as soon as the inner region unstable disk particles reach a temperature $T \gtrsim 17$ keV—the energy needed to populate the target particle orbits for Penrose Compton scattering, assuming, of course, the probable existence of turning points (compare eq. [1] and discussion in § 2), this Penrose process can "turn on" (Williams 2002b), irrespective of the mass of the rotating black hole. Moreover, the general observed high energy luminosity spectra of quasars and microquasars can be reproduced by these processes (see Williams 2002b, 2003). The above features are general characteristics of observed black hole sources. None of the 3-D MHD energy extraction jet models at the present (e.g., Koide et al. 2000; Meier et al. 2001; Koide et al. 2002; Koide 2003, 2004) exhibit such characteristic features in such details as does the Penrose-Williams mechanism. Nevertheless, 3-D MHD models can possible achieve the necessary powers (Blandford & Znajek 1977; Meier et al. 2001), but, in some cases, only after assuming an unrealistically large strength magnetic field.

Lastly, it appears that the modern-day Blandford-Znajek (1977) and Blandford-Payne (1982) type models are essentially faced with the age-old problem of converting from electromagnetic energy to particle energy and thus the inability of generating the highly relativistic particles needed to be consistent with observations. The problems associated with such models in the direct extraction of energy near the event horizon suggest that these models may be important in the weak gravitational field limit, serving perhaps the same purpose they do in the jets of protostars, i.e., appearing to have a dominant role on a large scale at distances outside the strong effects of general relativity. The recent model of Koide (2004) and its application to γ-ray bursts, assuming a large scale, superstrong radial magnetic field ($\sim 10^{15}$ G) down to the event horizon of a rapidly rotating KBH ($a = 0.99995$), produces a mildly relativistic outflow. Not only, at least at the present, does this model not collimate,

but it may not be consistent with the general relativistic determination that any "radiat-able" multipole field gets radiated away completely as a star collapses to a KBH (de la Cruz, Chase, & Israel 1970; Price 1972), which includes the magnetic field, leaving only nonzero monopole parameters M, J, and q, where J ($= Ma$) is the black-hole angular momentum, and q is the electric charge, hence the "no-hair theorem" (Misner, Thorne, & Wheeler 1973; Carter 1973). Also, the problem remains in the model of Koide (2004) as to how such a superstrong field is created in the popular (or generally accepted) model of stellar evolution.

In any case, the Penrose-Williams processes described in this paper (see also Williams 2002a, 2002b, 2003) may be related to the beamed energy output observed in γ-ray bursts. It is suspected that these processes, which could "quickly" turn on and off under suitable conditions, might be important. Particularly, these processes might prove to be invaluable in explaining the jets in so-called collapsars, i.e, black hole formation in massive stars with rotation (MacFadyen, Woosley, & Heger 2001), without the needed of a superstrong magnetic field. Equally, considering an "inactive" and/or perhaps "isolated" rotating black hole, if its tidal forces encounter and destroy an object of sufficient density, then as the debris is infalling, these Penrose processes could produce characteristics associated with some γ-ray bursts: an energetic short-lived burst, collimation, synchrotron emission, as well as the afterglows in the X-ray (Costa et al. 1997), optical (van Paradijs et al. 1997), and radio (Frail et al. 1997) regimes. That is, γ-ray and X-ray jets can be produced possibly from Penrose Compton scattering, and radio to optical synchrotron jet emission from subsequent Penrose pair production ($\gamma\gamma \longrightarrow e^- e^+$) electrons, interacting with the expected intrinsically induced magnetic field (mentioned above). Details of the application of these Penrose processes to γ-ray bursts await future investigations.

Note, in general, evaluation in a full-scale relativistic MHD regime is needed to follow the evolution of the trajectories of the escaping Penrose particles and their interactions with the intrinsically induced magnetic field and that of the surrounding accretion disk. This indeed will be a challenge. Yet, with existing MHD 3-D simulations, and since we have analytical expressions for the trajectories of the escaping particles (see Williams 2002a), such a task could be accomplished.

Finally, for completeness, even though the Penrose processes present here are quite efficient (Williams 1995) without a magnetic field, the presence of a disk magnetic field, however, inside the ergosphere, might increase the efficiency (see Wagh & Dadhich 1989 and references therein). The effects of such a magnetic field, if sufficiently small, might be represented by a random motion superimposed on the orbital velocities of the charged particles, say the target electrons in Penrose Compton scattering (see e.g. Williams 1995).

REFERENCES

Bardeen, J. M., Press, W. H., & Teukolsky, S. A. 1972, ApJ, 178, 347

Bičák, J. 2000, Pramana, 55, No. 4, 481 (gr-qc/0101091)

Bičák, J. & Ledvinka, T. 2000, IL Nuovo Cimento, 115 B, 739 (gr-qc/0012006)

Bičák, J., Semerák, O., & Hadrava, P. 1993, MNRAS, 263, 545

Blandford, R. D., & Payne, D. G. 1982, MNRAS, 199, 883

Blandford, R. D., & Znajek, R. L. 1977, MNRAS, 179, 433

Boyer, R. H., & Lindquist, R. W. 1967, J. Math. Phys., 8, 265

Carter, B. 1968, Phys. Rev., 174, 1559

Carter, B. 1973, in Black Holes, ed. C. DeWitt & B. S. DeWitt (New York: Gordon and Breach Science Publishers), 57

Costa, E. et al. 1997, Nature, 387, 783

de Felice, F., & Calvani, M. 1972, IL Nuovo Cimento, 10 B, 447

de Felice, F., & Carlotto, L. 1997, ApJ, 481, 116

de Felice, F., & Curir, A. 1992, Class. Quantum Grav., 9, 1303

de Felice, F., & Zanotti, O. 2000, Gen. Rel. Grav., 8, No. 32, 1449

Eilek, J. A. 1980, ApJ, 236, 664

Frail, D. A., Kulkarni, S. R., Nicastro, L., Feroci, M., & Taylor, G. B. 1997, Nature, 389, 261

Eilek, J. A., & Kafatos, M. 1983, ApJ, 271, 804

Gabuzda, D. C., & Murray, E. 2003, in Future Directions in High Resolution Astronomy: The 10th Anniversary of the VLBA, ed. J. D. Romney & M. J. Reid (astro-ph/0309668)

Homan, D. C. 2003, in Future Directions in High Resolution Astronomy: The 10th Anniversary of the VLBA, ed. J. D. Romney & M. J. Reid (astro-ph/0401320)

de la Cruz, V., Chase, J. E., & Israel, W. 1970, Phys. Rev. Lett., 24, 423

Junor, W., Biretta, J. A., & Livio, M 1999, Nature, 401, 891

Karas, V., & Dovčiak, M. 1997, Gen. Rel. Grav., 29, 1449

Kerr, R. P. 1963, Phys. Rev. Lett., 11, 237

Koide, S. 2003, Phys. Rev. D, 67, 104010

Koide, S. 2004, ApJ, 606, L45

Koide, S., Meier, D. L., Shibata, K., & Kudoh, T. 2000, ApJ, 536, 668

Koide, S., Shibata, K., Kudo, T., & Meier, D. L. 2002, Science, 295, 1688

Landau, L. D., & Lifshitz, E. M. 1975, The Classical Theory of Fields (Oxford: Pergamon Press)

Lightman, A. P., & Eardley, D. M. 1974, ApJ, 187, L1

MacFadyen, A. I., Woosley, S. E., & Heger, A. 2001, ApJ, 550, 410

Mahadevan, R., Narayan, R., & Krolik, J. 1997, ApJ, 486, 268

Meier, D. L., Koide, S., & Uchida, Y. 2001, Science, 291, 84

Misner, C. W., Thorne, K. S., & Wheeler, J. A. 1973, Gravitation (New York: W. H. Freeman and Company)

Novikov, I. D., & Thorne, K. S. 1973, in Black Holes, ed. C. DeWitt & B. S. DeWitt (New York: Gordon and Breach Science Publishers), 343

Penrose, R. 1969, Rivista Del Nuovo Cimento: Numero Speciale, 1, 252

Piran, T., & Shaham, J. 1977, Phys. Rev. D, 16, No. 6, 1615

Price, R. H. 1972, Phys. Rev. D, 5, 2419

Shapiro, S. L., Lightman, A. P., & Eardley, D. M. 1976, ApJ, 204, 187

Thirring, H., & Lense, J. 1918, Phys. Z., 19, 156

Thorne, K. S., Price, R. H., & Macdonald, D. A. 1986, Black Holes: The Membrane Paradigm (New Haven: Yale University Press)

van Paradijs, J. et al. 1997, Nature, 386, 686

Wagh, S. M., & Dadhich, N. 1989, Phys. Rep., 183, 137

Wilkins, D. C. 1972, Phys. Rev. D, 5, 814

Williams, R. K. 1991, Ph.D. thesis, Indiana Univ.

———. 1995, Phys. Rev. D, 51, 5387

———. 1999, in Proceedings of The Eighth Marcel Grossmann Meeting on General Relativity, Jerusalem, Israel, ed. T. Piran & R. Ruffini (Singapore: World Science), 416

———. 2001, in Relativistic Astrophysics: 20th Texas Symposium, Austin, Texas, ed. J. C. Wheeler & H. Martel (New York: American Institute of Physics), 448 (astro-ph/0111161)

———. 2002a, submitted to Phys. Rev. D (astro-ph/0203421)

———. 2002b, submitted to ApJ (astro-ph/0210139)

———. 2003, submitted to ApJ (astro-ph/0306135)

Wilms, J., Reynolds, C. S., Begelman, M. C., Reeves, J., Molendi, S., Staubert, R., & Kendziorra, E. 2001, MNRAS, 328, L27 (astro-ph/0110520)
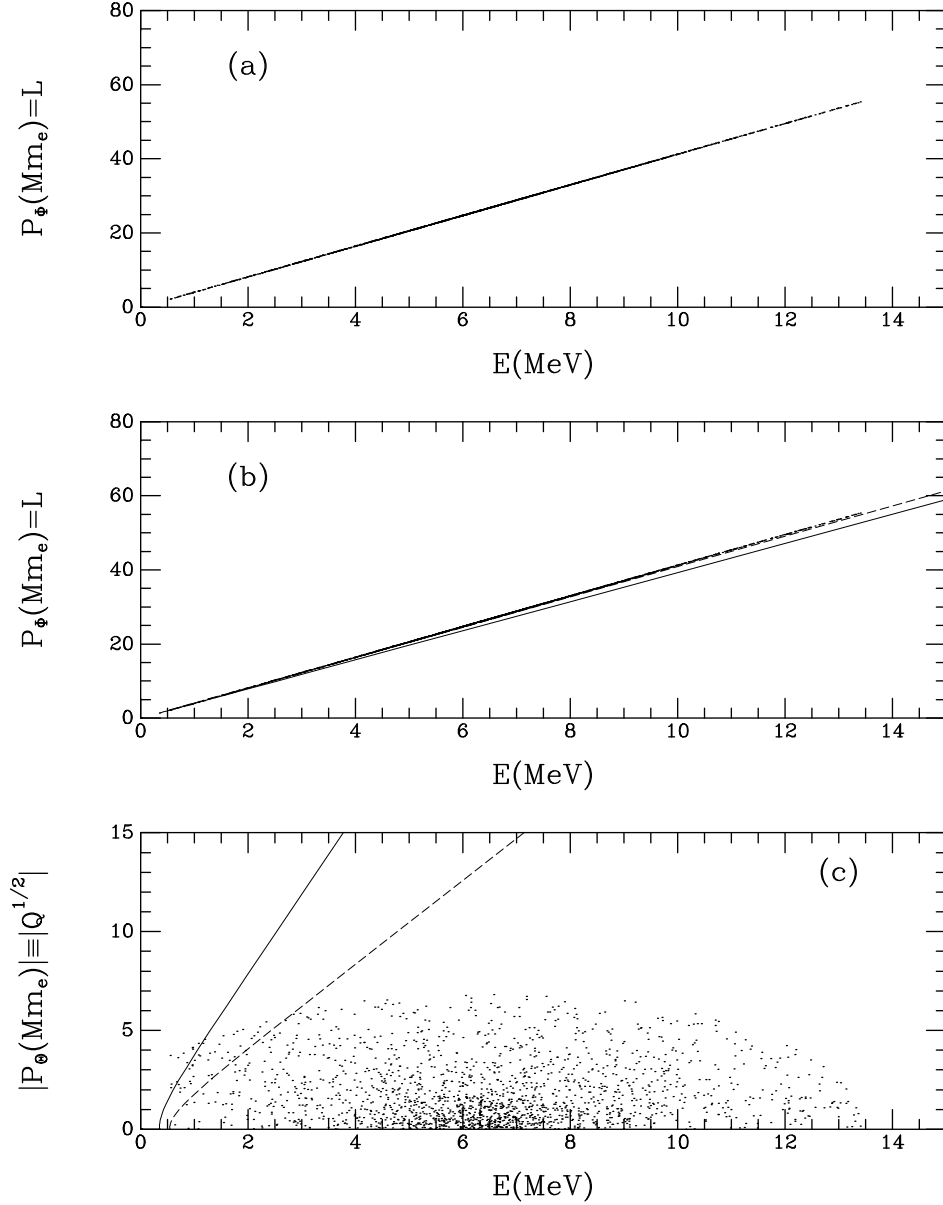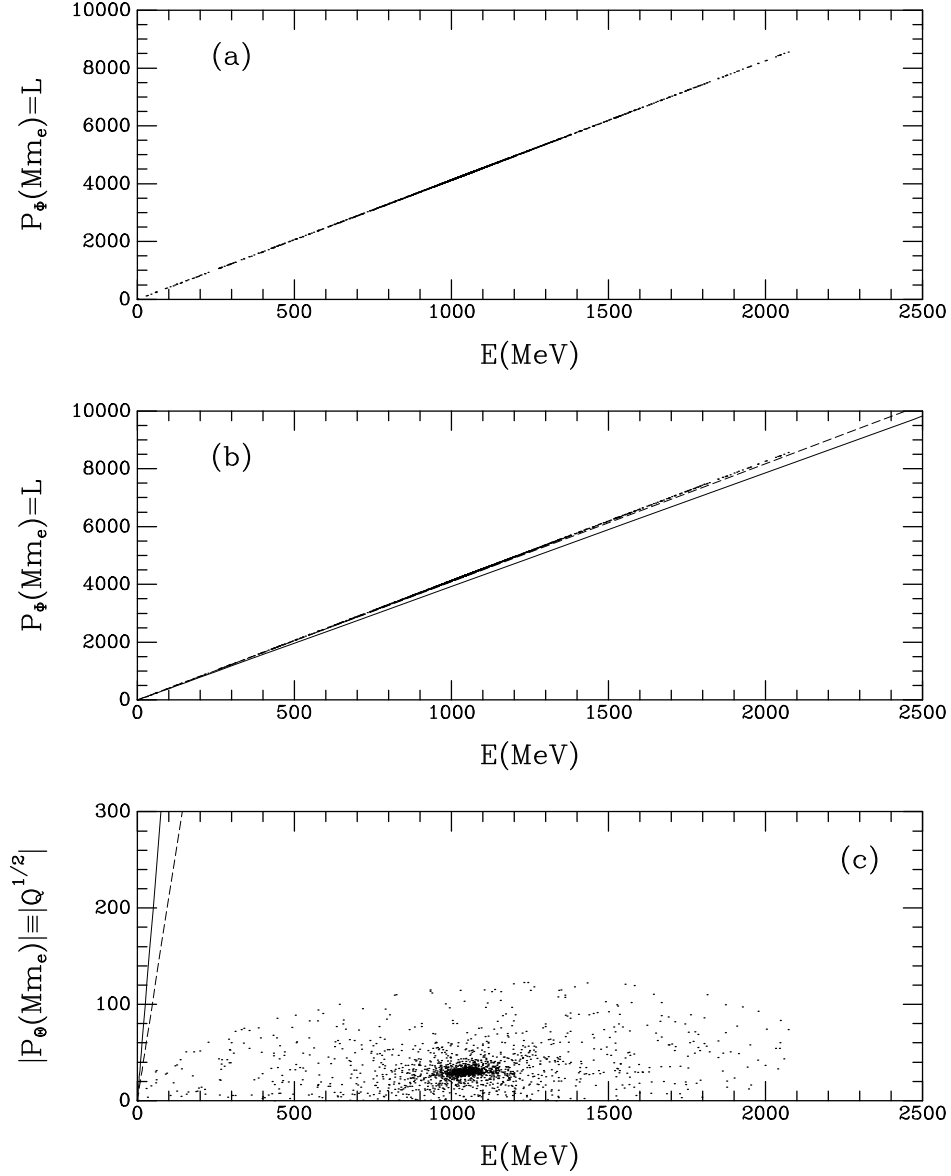
Fig. 1.— Magnitude of the azimuthal ($P_\Phi = L$) and polar (P_Θ) coordinate momenta for escaping vortical trajectories of electrons from Penrose pair production ($\gamma\gamma \longrightarrow e^-e^+$) at $r_{\rm ph} = 1.074M$, and for the bound nonequatorially confined electron particle orbits that cross the equatorial plane ($P_\Theta \equiv Q^{1/2}$): $(P_e)_\Phi$ vs. E_e and $(P_e)_\Theta$ vs. E_e, of electron orbits, at $r_{\rm mb} \simeq 1.089M$ (dashed curve) and at $r_{\rm ms} \simeq 1.2M$ (solid curve). (a) Scatter plot displaying $L_\mp$ vs. $E_\mp$ of e^-e^+ pairs after 2000 events (each point represents an escaping electron). The case shown has initial parameters: $E_{\gamma1} = 0.03$ MeV, the infalling photon energy; $E_{\gamma2} \simeq 13.54$ MeV, the target photon orbital energy; $L_{\gamma2} \simeq 55.6Mm_e$, corresponding azimuthal coordinate momentum; $Q_{\gamma2}^{1/2} = \pm0.393\,Mm_e$, corresponding polar coordinate momentum $(P_{\gamma2})_\Theta$; and $M = 10^8M_\odot$. (b) $L_\mp$ vs. $E_\mp$ superimposed on the orbital parameters L_e vs. E_e; see also Fig. 4. (c) $(P_\mp)_\Theta$ vs. $E_\mp$ superimposed on the orbital parameters $(P_e)_\Theta$ vs. E_e.

Fig. 2.— Magnitude of the azimuthal ($P_\Phi = L$) and polar (P_Θ) coordinate momenta for escaping vortical trajectories of electrons from Penrose pair production ($\gamma\gamma \longrightarrow e^-e^+$) at $r_{\rm ph} = 1.074M$, and for the bound nonequatorially confined electron particle orbits that cross the equatorial plane ($P_\Theta \equiv Q^{1/2}$): $(P_e)_\Phi$ vs. E_e and $(P_e)_\Theta$ vs. E_e, of electron orbits, at $r_{\rm mb} \simeq 1.089M$ (dashed curve) and at $r_{\rm ms} \simeq 1.2M$ (solid curve). (a) Scatter plots displaying $L_\mp$ vs. $E_\mp$ and $(P_\mp)_\Theta$ vs. $E_\mp$ of e^-e^+ pairs after 2000 events (each point represents an escaping electron). The case shown has initial parameters: $E_{\gamma 1} = 0.03$ MeV, the infalling photon energy; $E_{\gamma 2} \simeq 2146$ MeV, the target photon orbital energy; $L_{\gamma 2} \simeq 8.81 \times 10^3 Mm_e$, corresponding azimuthal coordinate momentum; $Q_{\gamma 2}^{1/2} = \pm 62.28 \, Mm_e$, corresponding polar coordinate momentum $(P_{\gamma 2})_\Theta$; and $M = 10^8 M_\odot$. (b) $L_\mp$ vs. $E_\mp$ superimposed on the orbital parameters L_e vs. E_e; see also Fig. 5. (c) $(P_\mp)_\Theta$ vs. $E_\mp$ superimposed on the orbital parameters $(P_e)_\Theta$ vs. E_e.
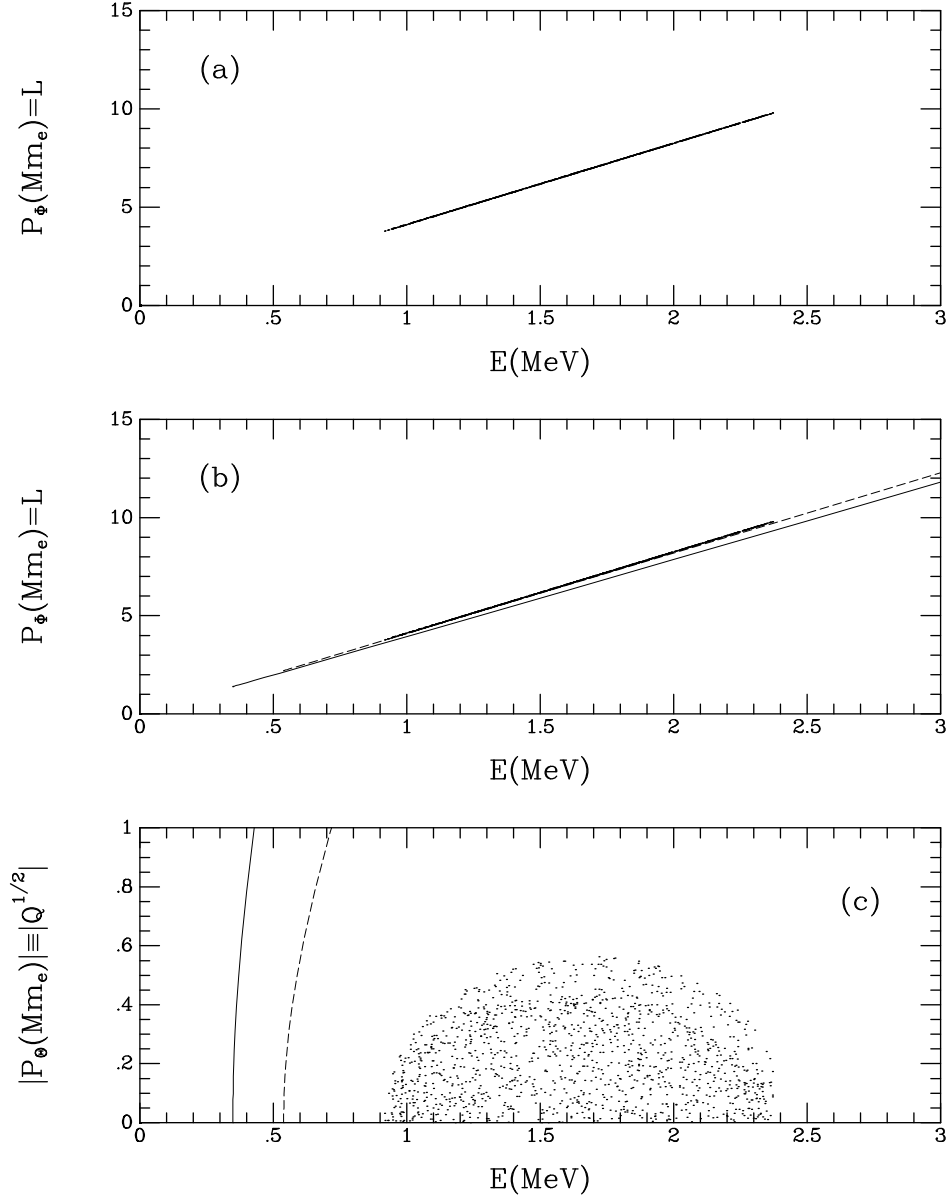
Fig. 3.— Magnitude of the azimuthal ($P_\Phi = L$) and polar (P_Θ) coordinate momenta for escaping vortical trajectories of electrons from Penrose pair production ($\gamma\gamma \longrightarrow e^- e^+$) at $r_{\rm ph} = 1.074M$, and for the bound nonequatorially confined electron particle orbits that cross the equatorial plane ($P_\Theta \equiv Q^{1/2}$): $(P_e)_\Phi$ vs. E_e and $(P_e)_\Theta$ vs. E_e, of electron orbits, at $r_{\rm mb} \simeq 1.089M$ (dashed curve) and at $r_{\rm ms} \simeq 1.2M$ (solid curve). (a) Scatter plots displaying $L_\mp$ vs. $E_\mp$ and $(P_\mp)_\Theta$ vs. $E_\mp$ of $e^- e^+$ pairs after 2000 events (each point represents an escaping electron). The case shown has initial parameters: $E_{\gamma 1} = 0.0035$ MeV, the infalling photon energy; $E_{\gamma 2} \simeq 3.387$ MeV, the target photon orbital energy; $L_{\gamma 2} \simeq 13.86 M m_e$, corresponding azimuthal coordinate momentum; $Q_{\gamma 2}^{1/2} = \pm 0.125 \, M m_e$, corresponding polar coordinate momentum $(P_{\gamma 2})_\Theta$; and $M = 30 M_\odot$. (b) $L_\mp$ vs. $E_\mp$ superimposed on the orbital parameters L_e vs. E_e. (c) $(P_\mp)_\Theta$ vs. $E_\mp$ superimposed on the orbital parameters $(P_e)_\Theta$ vs. E_e.
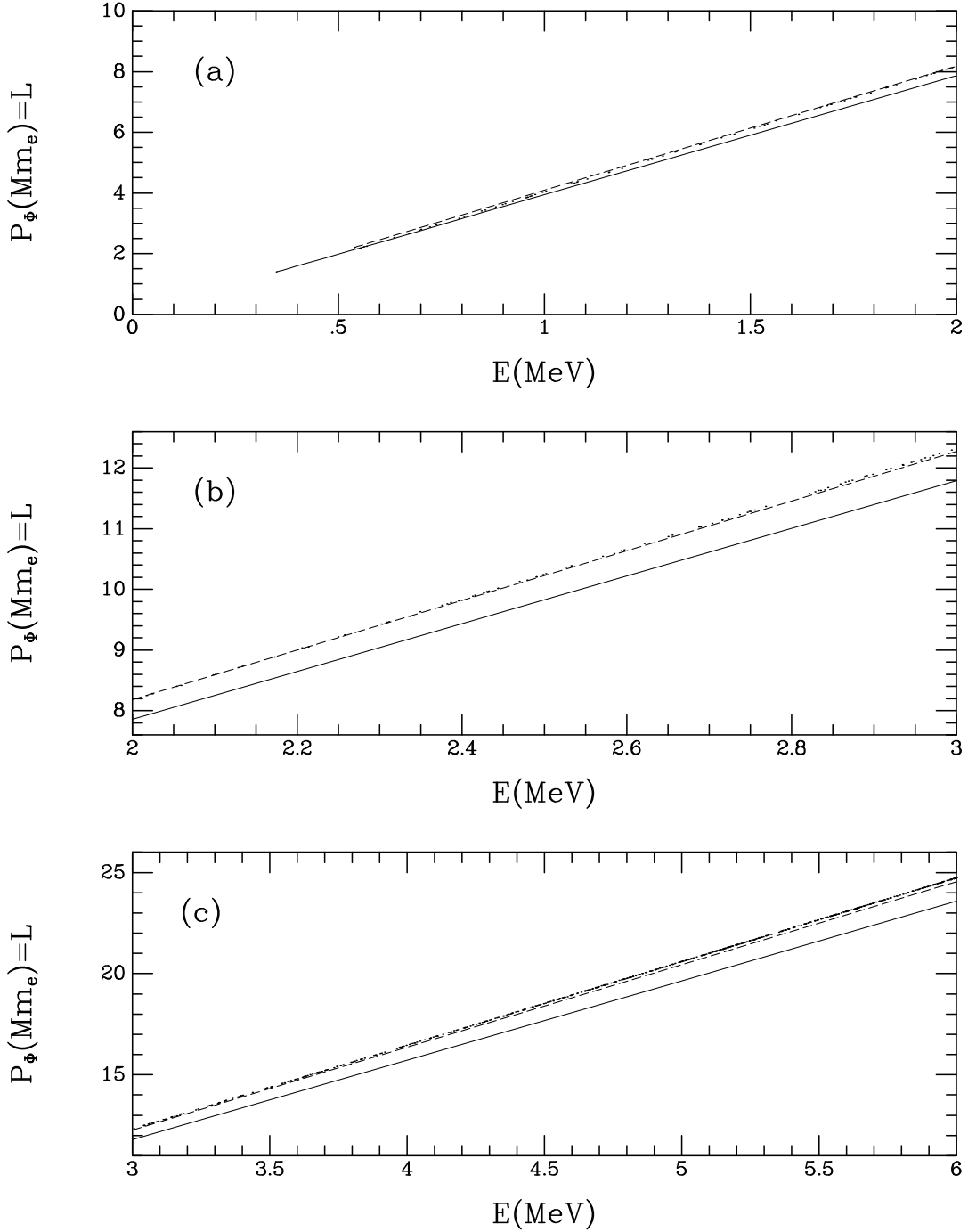
Fig. 4.— Magnitude of the azimuthal ($P_\Phi = L$) coordinate momentum for escaping vortical trajectories of electrons from Penrose pair production ($\gamma\gamma \longrightarrow e^- e^+$) at $r_{\rm ph} = 1.074M$ (scatter points), and for the bound nonequatorially confined electron particle orbits that cross the equatorial plane: $(P_e)_\Phi$ vs. E_e, of electron orbits, at $r_{\rm mb} \simeq 1.089M$ (dashed curve) and at $r_{\rm ms} \simeq 1.2M$ (solid curve). Panels (a), (b), and (c), showing $L_\mp$ vs. $E_\mp$, are specific intervals corresponding to Fig. 1b (see text).
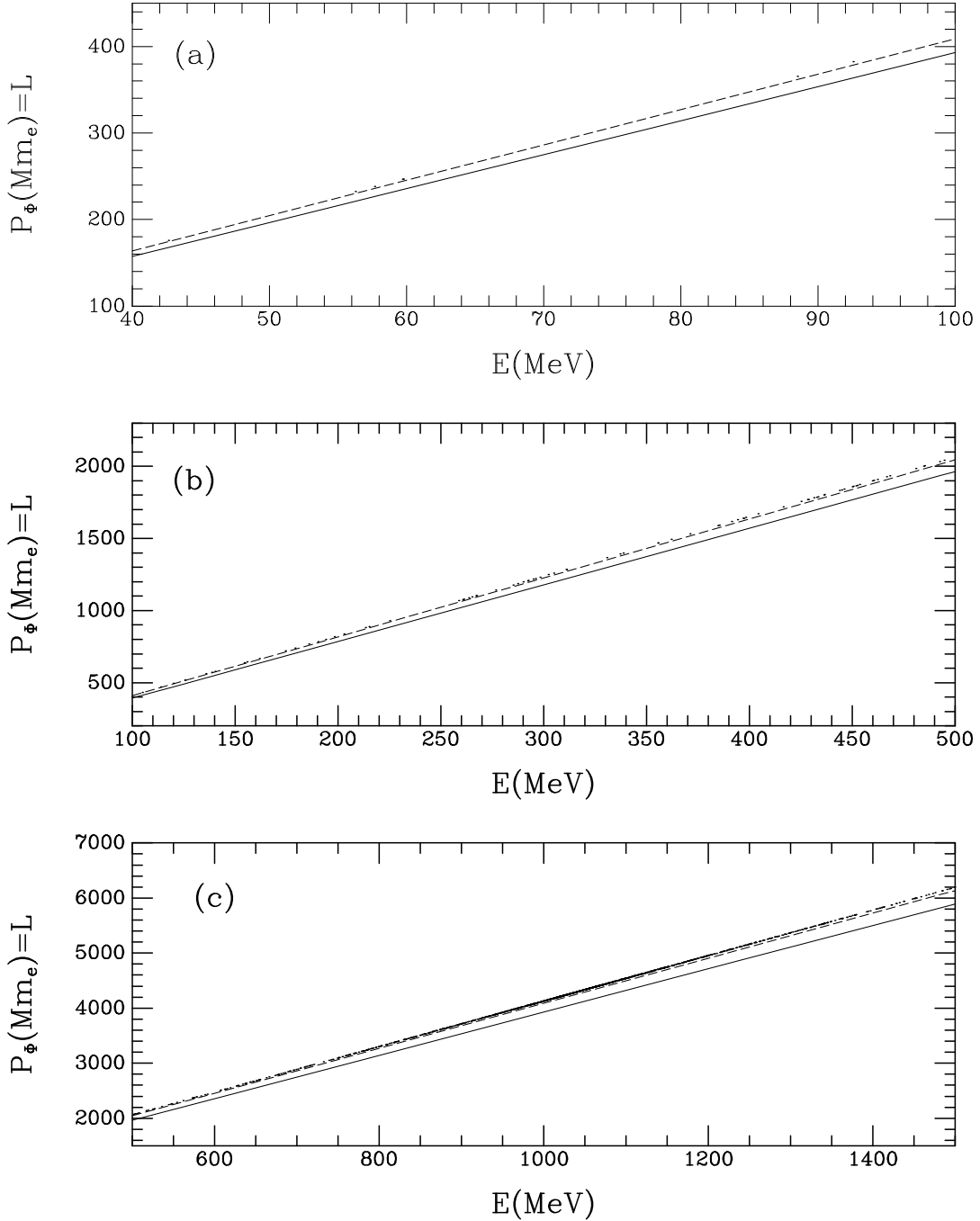
Fig. 5.— Magnitude of the azimuthal ($P_\Phi = L$) coordinate momentum for escaping vortical trajectories of electrons from Penrose pair production ($\gamma\gamma \longrightarrow e^-e^+$) at $r_{\rm ph} = 1.074M$ (scatter points), and for the bound nonequatorially confined electron particle orbits that cross the equatorial plane: $(P_e)_\Phi$ vs. E_e, of electron orbits, at $r_{\rm mb} \simeq 1.089M$ (dashed curve) and at $r_{\rm ms} \simeq 1.2M$ (solid curve). Panels (a), (b), and (c), showing $L_\mp$ vs. $E_\mp$, are specific intervals corresponding to Fig. 2b (see text).
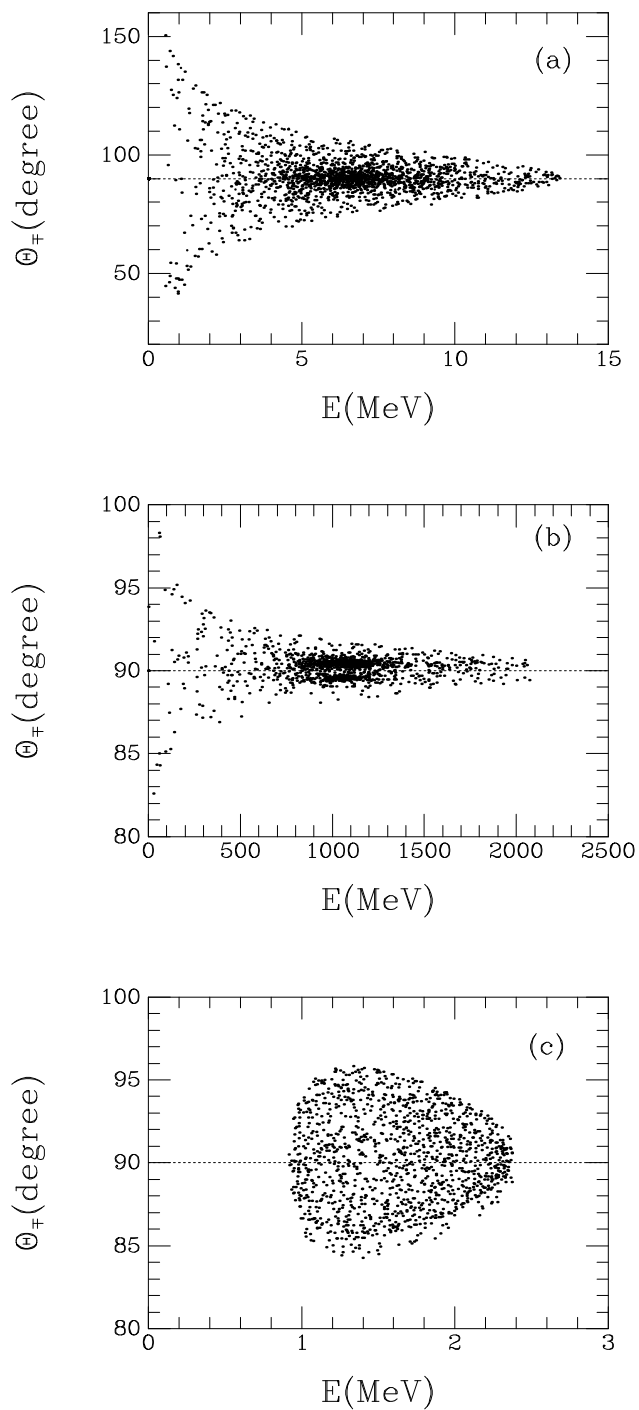
Fig. 6.— Penrose pair production ($\gamma\gamma \longrightarrow e^-e^+$): scatter plots displaying polar angles, above and below the equatorial plane ($\Theta = 90°$), for escaping e^-e^+ pairs (each point represents an electron). (a), (b), and (c), showing $\Theta_\mp$ vs. $E_\mp$, are the same as cases presented in Figs. 1, 2, and 3, respectively (see text).